Role of Phosphorus and Triethylene Glycol Incorporation on the Activity of Model Alumina-Supported CoMoS Hydrotreating Catalysts

Ricardo Garcia de Castro, Elodie Devers, Mathieu Digne, Anne-félicie Lamic-humblot, Gerhard Pirngruber, Xavier Carrier

Role of phosphorus and tri-ethylene glycol incorporation on the activity of model alumina-supported CoMoS hydrotreating catalysts

Dr. Ricardo GARCIA DE CASTRO,[1,2] Dr. Elodie DEVERS,[2] Dr. Mathieu DIGNE,[2] Dr. Anne-Félicie LAMIC-HUMBLOT,[1] Dr. Gerhard D. PIRNGRUBER,[2] Prof. Xavier CARRIER[1,*]

1- Sorbonne Université, CNRS, Laboratoire de Réactivité de Surface, 75005 Paris (France)

2- IFP Energies nouvelles, Rond-point de l'échangeur de Solaize, 69360 Solaize (France)

*xavier.carrier@sorbonne-universite.fr

Abstract

Environmental regulations concerning fuel-related sulfur emissions are currently experiencing worldwide expansion. This is motivating the research and development of improved hydrotreating (HDT) catalysts with carefully engineered synthesis methods that maximize activity as ultimate goal. In this contribution, the effect of phosphorus doping and triethylene glycol (TEG) incorporation on the genesis of the CoMoS phase of model HDT catalysts is assessed. Following a surface-science approach, α-Al_2O_3 single crystals with four orientations: C(0001), A($11\bar{2}0$), M($10\bar{1}0$), and R($1\bar{1}02$) are used as model supports of the traditional γ-Al_2O_3 support for the study of active phase-support interactions at the molecular scale. The model catalysts are prepared by traditional impregnation of a solution containing metal and phosphorus precursors and TEG. The catalysts are characterized in the sulfide phase by XPS, XAS, TEM, and AFM, revealing that the calcination step is key in the emergence of distinctive metal-support interactions, which are directly related to the nature of alumina surface sorption sites. In addition, TEG incorporation on dried catalysts increases metal sulfidation and enhances promotion with respect to non-additivated systems, especially at mild sulfidation temperatures. The catalytic activity of the model catalysts is tested in a thiophene hydrodesulfurization reaction, revealing the following activity trend with respect to alumina surface orientations: A($11\bar{2}0$) > > M($10\bar{1}0$) > R($1\bar{1}02$), C(0001). This trend is identical to the one observed for non-phosphorus doped non-TEG additivated model systems, confirming the predominance of surface effects on the catalytic activity over those exerted by P and TEG. By transposing these results to the industrial γ-Al_2O_3 support, the (100) facet would provide surface sites that lead to better performing catalysts. This could result in the development of novel supports, engineered to expose surface sites that maximize hydrotreating activity.

Introduction

The global demand for cleaner fuels has experienced a steady growth over the past decade since an increasing number of states have tightened their regulations related to the emission of atmospheric pollutants.[1] Special attention has been devoted to sulfur emissions, which are currently limited to 10 ppm for on-road fuels within members of the European Union.[2] It is expected that such restrictions will continue to expand worldwide in the following years. In such context, the demand for more efficient sulfur removal from fuels is driving the research and development of the concerned technologies. Industrial sulfur removal is better known as hydrotreating, a common oil refinery step devoted to heteroatom removal (S, N, O, heavy metals) via a catalytic reaction carried out by supported transition metal sulfides (e.g. Co-MoS_2/γ-Al_2O_3).[3,4] Consequently, many research efforts over the past six decades aimed at improving hydrotreating efficiency have been focused on the synthesis of better-performing catalysts.

Currently, there is consensus regarding the structure of the active phase in hydrotreating catalysts. The active phase is constituted of (pseudo)hexagonal MoS_2 slabs with cobalt decorating their edges, forming a mixed phase known as CoMoS.[3,5–7] These slabs are anchored to the support, suggesting a relationship between them. Several authors have confirmed such relationship, including the effect of support chemistry e.g. SiO_2, TiO_2, and Al_2O_3 polymorphs, on the properties of the active phase (sulfidation degree, slab length, stacking number, slab orientation relative to the support), with stronger metal-support interactions leading to higher active phase dispersion and lower sulfidation extents.[8,9]

Further research led to improve hydrotreating catalyst formulations by first incorporating phosphorus as dopant while the newest catalyst generation includes an organic additive (e.g. TEG) as well.[10–12] It has been proposed that the incorporation of phosphorus and organic additives weakens active phase-support interactions, especially in γ-Al_2O_3-supported catalysts, leading to higher sulfidation extents and ultimately to higher performances.[13,14]

However, despite the knowledge gathered on the active phase-support relationship over the past decades, the subject remains less understood at the molecular level. Indeed, γ-Al_2O_3 (the industrial support) is a polycrystalline material that exhibits numerous different sorption sites (surface -OH groups).[15] Therefore, the influence of specific sorption sites on the genesis of the active phase is still unclear due to the nature of the support itself. In order to circumvent the structural complexity of polycrystalline systems, reductionist approaches based on the use of

single crystals as model supports have been recently explored.[16–19]. For instance, Bara et al.[20,21] used α-Al_2O_3 single crystals of four different orientations: C(0001), A($11\bar{2}0$), M($10\bar{1}0$) and R($1\bar{1}02$) as model supports in order to exert control over the speciation of surface sites. α-Al_2O_3 is used as a surrogate for γ-Al_2O_3 since no macroscopic single crystal can be prepared with transition γ-Al_2O_3. α-Al_2O_3 crystal planes have well-defined surface -OH speciation, which has been the subject of experimental and theoretical research over the past decades. Interestingly, various studies in this field suggest that α- and γ-Al_2O_3 crystal planes share common surface sorption sites[22] which implies that α-Al_2O_3 single crystals can be used as model supports for the study of hydrotreating catalysts at the molecular level. Results obtained for these model systems can then be transposed to real γ-Al_2O_3-based catalysts by comparison of common surface -OH groups on both polymorphs. Nonetheless, it must be stated that the nature of surface sorption sites for both α- and γ-Al_2O_3 is still highly debated, so the α- / γ– analogy might evolve with improved evidence on the nature of the γ-Al_2O_3 surface structure.[15]

The work of Bara *et al*.[20,21] demonstrated that the genesis of the active phase is surface-dependent, with different surface sites leading to characteristic trends in sulfidation extent and Mo dispersion. More recent contributions sought to bridge the gap between model and industrial hydrotreating catalysts by studying the surface-dependent nature of phosphorus doping and cobalt promotion under such approach.[23,24] These studies not only revealed a surface-dependent interaction of phosphorus precursors with the support, but most remarkably, that intrinsic hydrodesulfurization activity of Co-promoted catalysts is surface-dependent, with active phase-support interactions of intermediate strength leading to the highest catalytic activity.[23,24]

In this work, we propose a step further in closing the gap between model systems and real catalysts through the simultaneous incorporation of both Co and P on the formulation of model catalysts supported on the C(0001), A($11\bar{2}0$), M($10\bar{1}0$) and R($1\bar{1}02$) α-Al_2O_3 planes. In addition, the incorporation of an organic additive (triethylene glycol, TEG) in the formulation is discussed as well. In that sense, this contribution seeks to give a comprehensive view of the effect exerted by surface sorption sites on the properties and performance of model hydrotreating catalysts prepared with typical industrial formulations. For that, model P-doped CoMoS/α-Al_2O_3 catalysts were synthesized by aqueous-phase deposition of active components and further analyzed in the sulfide state by XPS, XANES (metal sulfidation), AFM and TEM (active phase dispersion). At last, the activity of the model catalysts was evaluated through a

thiophene hydrodesulfurization reaction in order to relate the genesis of the active phase to their intrinsic activity.

Results

Effect of the calcination step on impregnated CoMoP samples: dried vs. calcined catalysts

The influence of the calcination step on the sulfidation and promotion extents of model CoMoP catalysts was studied to better understand its effect on active phase-support interactions and the genesis of the promoted active phase. Dried CoMoP catalysts will be later compared to CoMoP-TEG catalysts, which were prepared omitting the calcination step. Thus, in order to identify the effect of TEG, the impact of the calcination step on metal sulfidation should be discerned beforehand. In addition, in order to study the impact of phosphorus on the genesis of the promoted active phase in calcined catalysts, both average sulfidation and promotion extents from CoMo catalysts (reported in a previous contribution[23]) will be confronted to those of CoMoP catalysts. Such descriptors were obtained through XPS analysis of model catalysts sulfided at 300 °C and 400 °C (Fig. 1).

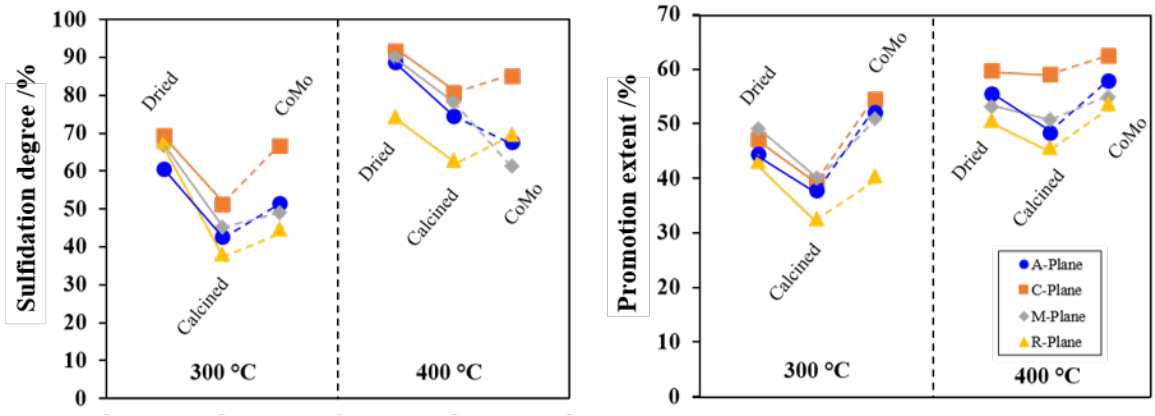

Figure 1. Sulfidation degree (left) and promotion extent (right) of dried and calcined model CoMoP catalysts supported on the C(0001), A(11$\bar{2}$0), M(10$\bar{1}$0) and R(1$\bar{1}$02) planes of α-Al_2O_3 prepared by impregnation from a solution with P/Mo = 0.57 and Co/Mo = 0.5 sulfided at 300 and 400 °C. Sulfidation and promotion extents of calcined model CoMo catalysts without P prepared by impregnation (Co/Mo = 0.5[23]) are presented as reference (marked as CoMo in the Figure).

Results from Fig. 1 show that dried samples exhibit higher sulfidation degrees than calcined CoMoP samples, regardless of the crystal plane and the sulfidation temperature. At 300 °C, the sulfidation extent of dried samples is 18% to 30% higher than that of calcined

catalysts, depending on the model surface. However, this difference narrows down to 11-14% at 400 °C sulfidation, suggesting that dried catalysts sulfide easier than calcined ones, as already remarked by van Haandel *et al*.[25]

The promotion extent of calcined CoMoP catalysts is also consistently lower than that of dried CoMoP catalysts (except for the C(0001) plane at 400 °C). This is probably a direct consequence of the higher sulfidation degrees reported on dried catalysts, since cobalt edge decoration is directly related to the availability of MoS_2 species, as discussed in Ref.[23] Therefore, for fixed sulfidation conditions, we conclude that CoMoP catalyst calcination leads to a decrease of both sulfidation degree and promotion extent, which can be related to stronger metal-support interactions upon calcination. High sulfidation temperature tends to level these effects.

Reference CoMo catalysts prepared by impregnation were incorporated in Fig.1 in order to assess the effect of P-doping on Mo and Co sulfidation in calcined catalysts. As seen in Fig. 1 (left), the Mo sulfidation degrees of model calcined CoMoP catalysts at 300 °C sulfidation are lower than those of reference CoMo catalysts, regardless of the crystal plane. Indeed, Mo sulfidation decreases 8-16% in the presence of phosphorus at P/Mo = 0.57, in line with a previous work involving non-promoted P-doped model catalysts.[24] The results at 400 °C are less conclusive as such behavior is only found for C(0001) and R($1\bar{1}02$)-based catalysts. The composite interplay between phosphorus addition and temperature on sulfidation degree leads to a less conclusive trend at 400°C for the A($11\bar{2}0$) and M($10\bar{1}0$) planes, which are described as surfaces with medium active-phase support interactions. It may then be concluded that at high sulfidation temperatures (400°C), temperature will moderate any effects caused by phosphorus in active phase-support interactions.

Fig. 1 (right) also shows consistently lower promotion extents at 300 °C sulfidation in the presence of phosphorus, in line with a direct correlation between sulfidation and promotion extents discussed in Ref.[23] Again, these differences are less pronounced at 400 °C due to overall higher Mo sulfidation degrees at this activation temperature. In conclusion, the incorporation of phosphorus visibly delays both sulfidation and promotion extents at 300 °C sulfidation, while activation at 400 °C appears to level out such effect.

Effect of triethylene glycol incorporation on dried model catalysts prepared by impregnation

Mo-Sulfidation and Co-promotion

The effect of triethylene glycol on Mo sulfidation and Co promotion of model dried CoMoP catalysts was studied at 300 and 400 °C. In this case, the calcination step was omitted to preserve the integrity of TEG before sulfidation since TEG thermally decomposes above 200 °C [26] and all TEG would have disappeared from the calcined surface before a 300 °C sulfidation. This procedure has been followed by similar studies.[12,25,27] To corroborate this, the disappearance of TEG after 300 °C sulfidation was verified by XPS analysis (C1s spectra before and after sulfidation are available in the Supporting Information).

The sulfidation and promotion extents of TEG-additivated catalysts are compared in Fig. 2 to those obtained for non-additivated dried CoMoP samples.

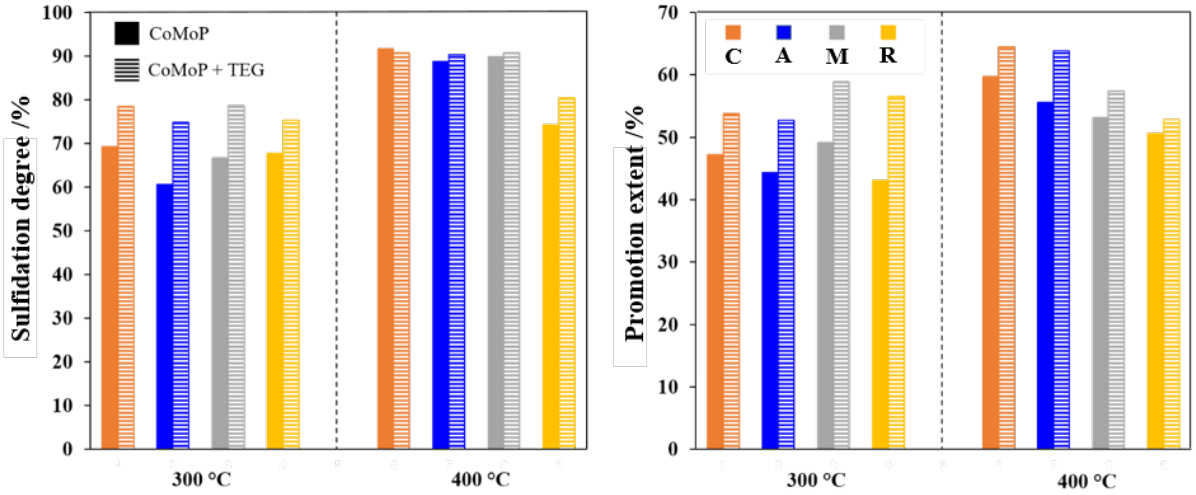

Figure 2. Mo Sulfidation (left) and Co promotion extents (right) at 300 and 400 °C sulfidation of dried model CoMoP and CoMoP additivated with TEG catalysts (P/Mo = 0.57, Co/Mo = 0.5) supported on the C(0001), A(11$\bar{2}$0), M(10$\bar{1}$0) and R(1$\bar{1}$02) planes of α-Al_2O_3 prepared by impregnation.

As seen in Fig. 2 (left), CoMoP-TEG model catalysts supported on the C(0001), A(11$\bar{2}$0), M(10$\bar{1}$0) and R(1$\bar{1}$02) planes respectively display 9, 14, 12 and 8% higher Mo sulfidation extent than their CoMoP counterparts at 300 °C sulfidation. At 400 °C, these differences are notably reduced, except for R(1$\bar{1}$02) plane-based catalysts, which still display 6% more MoS_2 on TEG-additivated catalysts. These results suggest that TEG allows a more extensive Mo sulfidation at lower temperatures (300 °C), compared to CoMoP, CoMo (calcined, Ref. [23]) and MoP model

catalysts.[24] This sulfidation enhancement pinpoints to a reduction in metal-support interactions in CoMoP-TEG catalysts, allowing a more extensive Mo sulfidation at milder conditions.

Fig 2. (right) also reveals an enhancing effect of TEG on cobalt promotion for all model catalysts: this is especially true at 300 °C and promotion enhancement remains noticeable at 400 °C. XANES Co K-edge spectra acquired in Grazing-Incidence geometry of CoMoP and CoMoP-TEG model catalysts supported on the C(0001) and R($1\bar{1}02$) planes (Fig. 3) confirmed these results. The spectra show incomplete Co sulfidation at 300°C as the four spectra display features associated to both sulfidic and oxidic cobalt, in agreement with Nicosia and Prins.[12] For instance, the position of the oxidic Co^{2+} white line at around 7724 eV is shared by the four recorded spectra displayed in Fig. 3. Conversely, the presence of a distinct pre-edge (7709 eV) as well as the onset of the edge aligned with the shoulder of Co_9S_8 (7717 eV) on the four experimental spectra suggests the presence of a sulfide phase.[10] Co_9S_8 is taken as a reference of a sulfide phase as a general term since XANES can hardly discriminate Co atoms in either Co_9S_8 or a CoMoS phase, although a chemometric analysis method has been recently developed to extract the CoMoS contribution from EXAFS spectra of CoMo catalysts.[28] Linear combination fitting of the XANES spectra of the model catalysts on the C(0001) and R($1\bar{1}02$) planes using Co_9S_8 and oxidic Co^{2+} reference spectra (Fig. 3) allowed to calculate approximate percentages of cobalt in the sulfide (Co_9S_8 and CoMoS) and oxide phases. The results were compared to those obtained by XPS (Table 1). Although the cobalt sulfidation extents obtained by XPS are consistently higher than those obtained by XAS, both methods show an increase in Co sulfidation on CoMoP-TEG catalysts at 300 °C.

Table 1. Percentage of cobalt in the sulfide state (Co_9S_8 + CoMoS) obtained by XANES and XPS on model planar catalysts (dried CoMoP and CoMoP-TEG formulations) supported on the C(0001) and R($1\bar{1}02$) planes of α-Al_2O_3 prepared by impregnation and sulfided at 300 °C.

% Co as sulfide	C(0001)		R($1\bar{1}02$)	
	CoMoP	CoMoP+TEG	CoMoP	CoMoP+TEG
XPS	58.9	69.5	57.9	67.7
XAS	50.9	56.3	46.5	51.3

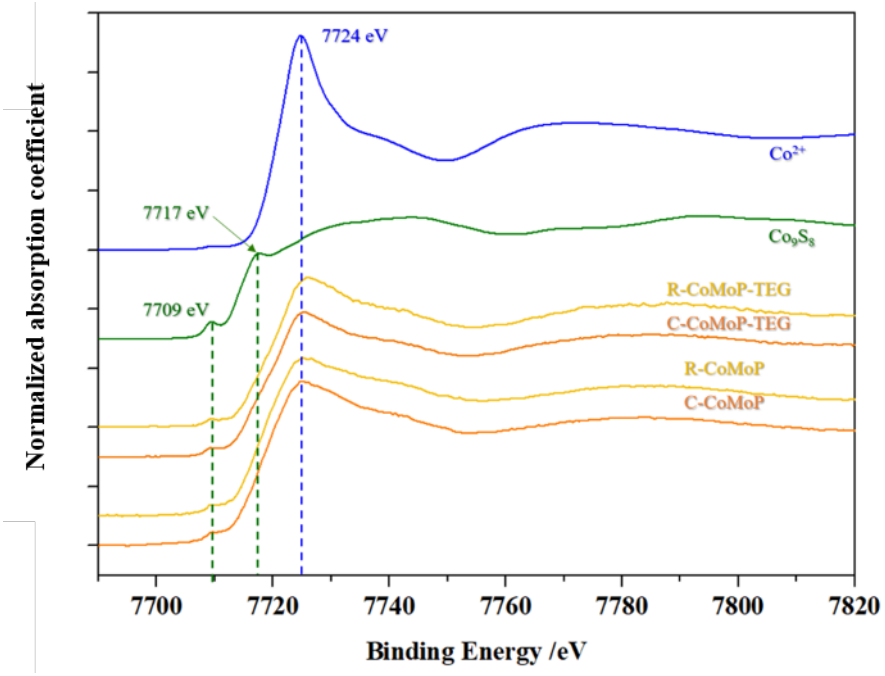

Figure 3. XANES Co K-edge spectra of model dried CoMoP and CoMoP-TEG catalysts supported on the C(0001) and R(1$\bar{1}$02) planes of α-Al_2O_3 prepared by impregnation and sulfided at 300 °C. Spectra were acquired in a parallel orientation of the electric field vector of the synchrotron beam relative to the wafer surface.

Gutierrez-Alejandre *et al.*[29] suggested that TEG is mainly adsorbed on defects on the surface of porous γ-Al_2O_3, where the strongest Lewis sites are located, and also on hydroxyl groups with higher vibrational frequency (e.g. monocoordinated -OH). This forces metal precursors to migrate to weaker-interacting sorption sites, resulting in higher sulfidation extents. In the case of model planar catalysts, the occurrence of defects is minimal, as suggested by AFM imaging of clean wafers of all four crystal orientations (See Supporting Information). However, single crystals exhibit defined Al-OH surface sorption sites with metal/support interactions of diverse nature as previously shown.[20,21,23,24] For instance, R(1$\bar{1}$02) plane-based catalysts exhibit mainly Al_{4c}-μ_1-OH sites, responsible for strong metal-support interactions, while C(0001) plane-based ones display Al_{6c}-μ_2-OH sites, associated to weaker interactions.[20,21,23,24] In that sense, we would expect a more significant effect of TEG on the R(1$\bar{1}$02) plane. Indeed, TEG R(1$\bar{1}$02)-based catalysts still display larger sulfidation extents at 400 °C compared to its additive-free counterpart, while differences are weaker for the other orientations at this temperature. However, results in Fig. 2 show that TEG incorporation lowers metal-support interactions for all surface orientations when sulfided at milder temperatures (300 °C).

TEG-additivated catalysts also exhibit a notorious enhancement in Co promotion extent at 300 °C sulfidation with respect to CoMoP catalysts, with 8, 7, 10 and 13% more Co in the CoMoS phase on planes A($11\bar{2}0$), C(0001), M($10\bar{1}0$) and R($1\bar{1}02$) respectively (Fig. 2, right). The enhancing effect of TEG remains noticeable at 400 °C but is reduced, as the differences between both catalyst formulations are narrowed to 8, 5, 4 and 2% more CoMoS phase for A($11\bar{2}0$), C(0001), M($10\bar{1}0$) and R($1\bar{1}02$) planes respectively. These results are in line with Mo sulfidation trends observed at 400°C on both catalyst formulations. This generalized increase in promotion extents is following the increase in Mo sulfidation upon TEG additivation, as it was previously shown that Co promotion is intimately related to Mo sulfidation.[23]

However, TEG additivation might also provide additional enhancing effects on Co promotion, which have been discussed in the literature. First, it has been suggested that TEG and other ethylene glycols delay both Mo and Co sulfidation up to 250 °C.[14,25,30] After that temperature, sulfidation would be fast, peaking at lower temperatures compared to CoMoP catalysts. This delay would allow simultaneous sulfidation of both transition metals and avoid the formation of refractory cobalt sulfides, which already constitute around 15% of cobalt species in model calcined CoMo catalysts sulfided at 200 °C.[23] In addition, Costa et al.[31] observed that TEG incorporation favored the formation of the bimetallic Keggin-type heteropolyanion $PCoMo_{11}O_{40}^{7-}$ at P/Mo molar ratios in solution above 0.4, in contrast with analogous TEG-free precursor solutions. The presence of this species in solution could be decisive for catalytic performance, since it would allow Mo and Co atoms to be adsorbed in proximity upon impregnation, allowing a more efficient decoration of MoS_2 slabs by Co, which would reduce the concentration of Co refractory phases, eventually increasing the promotion extent.[32,33]

To summarize, TEG incorporation allows higher sulfidation degrees due to reduced active phase-support interactions, which also certainly lead to an enhancement of the promotion extent given the intimate relationship between sulfidation and promotion. In addition, TEG is also presumably delaying both Co and Mo sulfidation and allowing the formation of $PCoMo_{11}O_{40}^{7-}$ at high P contents at the same time, ensuring a more efficient MoS_2 edge decoration and consequently increasing Co promotion.

Dispersion

A largely discussed role of TEG on the genesis of the CoMoS phase in porous catalysts is its enhancement of metal dispersion.[14,31] In order to evaluate this effect on model planar catalysts, XPS, AFM and TEM were used to assess metal dispersion in the sulfide state.

Mo/Al, Co/Al and P/Al surface atomic ratios were obtained from XPS analysis of the Mo3d, Co2p, P2p and Al2p regions (Table 2). The results show that both Mo/Al and Co/Al ratios increase in catalysts prepared with TEG, confirming that the incorporation of the organic additive enhances metal dispersion in planar systems, in agreement with similar studies.[14,27,30]

Table 2. Mo/Al, Co/Al and P/Al surface ratios obtained from I_{Mo3d}, I_{Co2p}, I_{P2p} and I_{Al2p} XPS regions of dried model CoMoP and CoMoP-TEG catalysts supported on the C(0001), A$(11\bar{2}0)$, M$(10\bar{1}0)$ and R$(1\bar{1}02)$ crystal planes of α-Al_2O_3 analyzed after sulfidation at 300 °C.

Plane	CoMoP			CoMoP+TEG		
	Mo/Al	Co/Al	P/Al	Mo/Al	Co/Al	P/Al
C	0.62	0.23	0.06	0.70	0.42	0.04
A	0.59	0.25	0.11	0.71	0.40	0.06
M	0.66	0.30	0.07	0.75	0.32	0.07
R	0.67	0.28	0.17	0.71	0.40	0.14

Conversely, the P/Al ratio is moderately affected by TEG addition. However, it is worth noticing that R$(1\bar{1}02)$ plane-based catalysts still display the highest P/Al ratio, even after TEG additivation, indicating consistently strong phosphate-support interactions, in agreement with non-promoted, non-additivated model catalysts.[24]

Another way to evaluate metal dispersion is by studying the surface topography by AFM imaging (Images available in Supporting Information) in order to determine the surface roughness (Table 3).

Table 3. Root mean square surface roughness (R_{rms}) of dried CoMoP and CoMoP-TEG model catalysts sulfided at 300 °C, supported on the C(0001), A$(11\bar{2}0)$, M$(10\bar{1}0)$ and R$(1\bar{1}02)$ planes of α-Al_2O_3 prepared by impregnation obtained via AFM measurements at a scale of 2 μm x 2 μm.

R_{rms}/ nm	CoMoP	CoMoP - TEG
C(0001)	0.89	0.64
A$(11\bar{2}0)$	0.62	0.49
M$(10\bar{1}0)$	0.56	0.47
R$(1\bar{1}02)$	0.39	0.32

As seen in Table 3, surface roughness increases in the order R$(1\bar{1}02)$ < M$(10\bar{1}0)$ < A$(11\bar{2}0)$ < C(0001) regardless of catalyst formulation. In addition, Table 3 shows that a decrease in surface roughness (i.e. indicating an increase in overall dispersion) is achieved upon TEG incorporation, in line with XPS results (Table 2).

The slab length and stacking number of the CoMoS slabs was studied via TEM for model catalysts supported on the four crystal planes prepared with both CoMoP and CoMoP-TEG formulations. The average slab length and stacking number are directly related to the dispersion degree and are descriptors used to rationalize changes in activity upon modification of the catalyst formulation. TEM images (Fig. 4) were posteriorly analyzed in order to perform statistical analysis of the slab length and stacking number (Fig. 5 and 6) for each formulation. TEM imaging was carried out using samples sulfided at 400 °C since the thiophene hydrodesulfurization reaction (section 3.3) was carried out at this temperature, and the calculation of a normalized conversion requires data obtained at the same temperature. A recapitulative table of TEM results is available at the end of this section (Table 4).

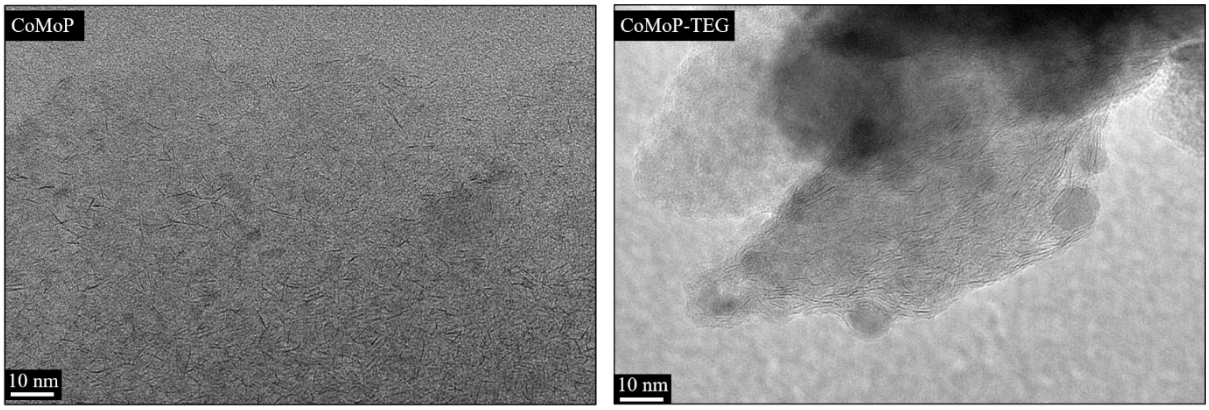

Figure 4. Representative TEM images of model dried CoMoP (left) and CoMoP+TEG (right) catalysts supported on the R(1$\bar{1}$02) plane of α-Al_2O_3 sulfided at 400 °C.

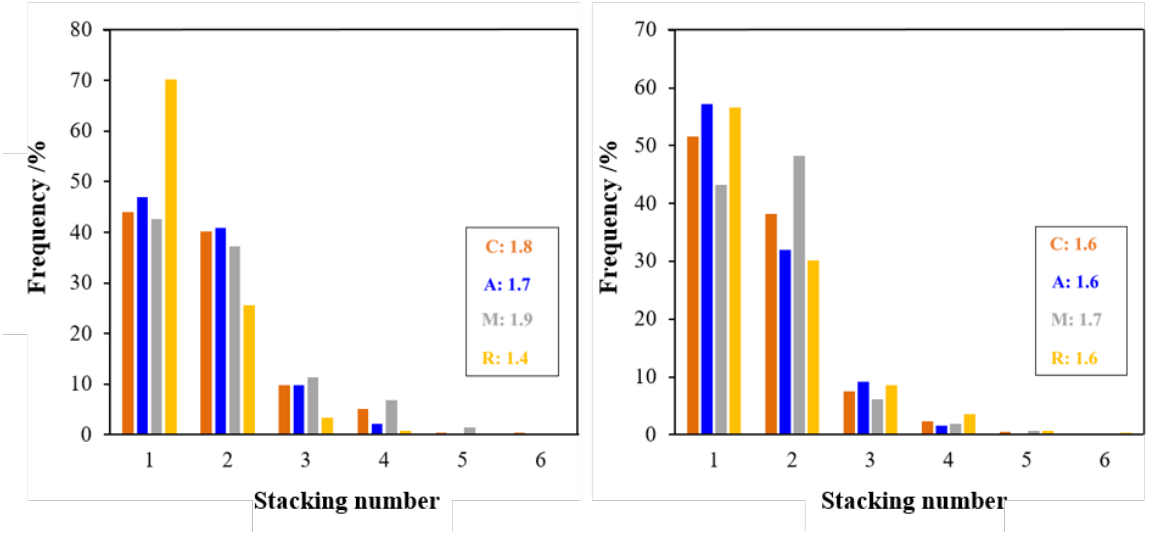

Figure 5. Stacking number distribution for dried model CoMoP (left) and CoMoP+TEG (right) catalysts supported on the C(0001), A(11$\bar{2}$0), M(10$\bar{1}$0) and R(1$\bar{1}$02) crystal planes of α-Al_2O_3 sulfided at 400 °C obtained via TEM image analysis.

As seen in Table 4, the average stacking number of CoMoP catalysts ranges from 1.4 (R(1$\bar{1}$02)-based) to 1.9 for (M(10$\bar{1}$0)-based). Upon TEG addition, a slight homogenization of the stacking number is noted, with an average of 1.6 for A(11$\bar{2}$0), C(0001) and R(1$\bar{1}$02) plane-based catalysts and 1.7 for M(10$\bar{1}$0)-based. This homogenization may be explained by a diffusion-limited growth of MoS_2 nanoparticles at the start of the sulfidation imposed by TEG molecules, leading to a leveling of the differences on different alumina orientations. A similar effect was also invoked for phosphorus on the same systems.[24] Nonetheless, the influence of TEG on stacking appears to be minor overall, in agreement with Mazoyer *et al.*[30] However, it has to be mentioned that another study found an important increase in the population of single

slabs upon TEG incorporation on CoMoP catalysts (63% vs. 44%)[34] which is not observed in our results.

The slab length distribution of supported CoMoS particles was also obtained from TEM imaging (Fig. 6). The effect of TEG on this descriptor is also marginal for the four surfaces (see also Table 4), with a slight tendency towards homogenization after additivation. The differences in slab length distribution were more pronounced (1 nm) among the various alumina orientations for calcined (non additivated) CoMo catalysts.[23]

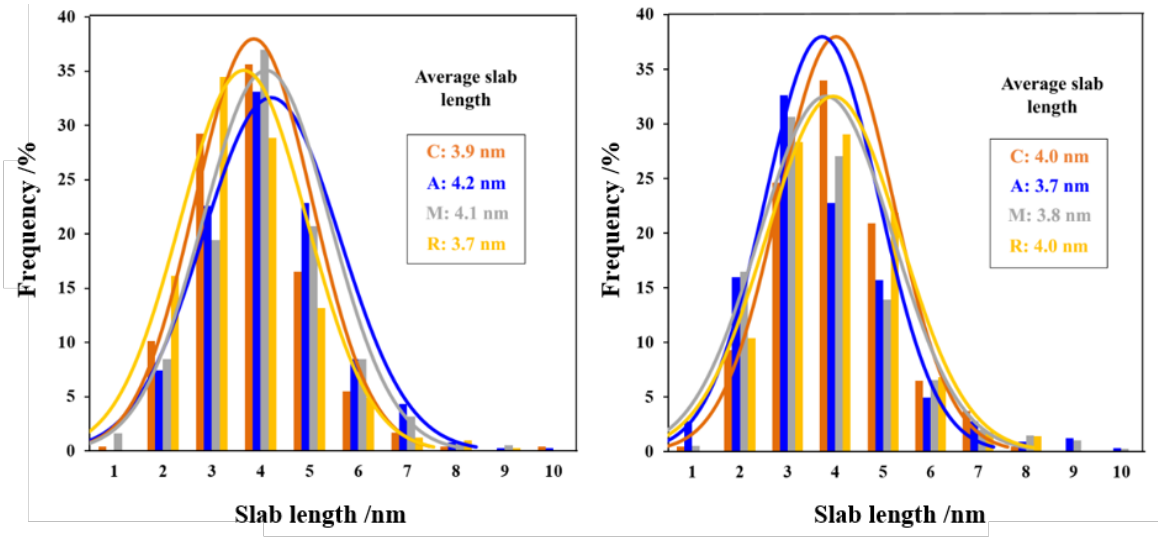

Figure 6. MoS_2 slab length distribution for dried model CoMoP (left) and CoMoP+TEG (right) catalysts supported on the C(0001), A($11\bar{2}0$), M($10\bar{1}0$) and R($1\bar{1}02$) crystal planes of α-Al_2O_3 sulfided at 400 °C obtained via TEM image analysis.

Table 4. Average stacking number, slab length and relative percentage of single slabs present in model catalysts supported on the C(0001), A($11\bar{2}0$), M($10\bar{1}0$) and R($1\bar{1}02$) crystal planes of α-Al_2O_3 sulfided at 400 °C prepared under the CoMo (calcined)[23], dried CoMoP and dried CoMoP-TEG formulations.

Plane	Average stacking number			Average slab length /nm			% Single slabs		
	CoMo	CoMoP	CoMoP-TEG	CoMo	CoMoP	CoMoP-TEG	CoMo	CoMoP	CoMoP-TEG
C	2.6	1.8	1.6	4.5	3.9	4.0	15%	44%	57%
A	2.2	1.7	1.6	3.9	4.2	3.7	26%	47%	51%
M	2.3	1.9	1.7	3.8	4.1	3.8	22%	43%	43%
R	1.7	1.4	1.6	3.5	3.7	4.0	51%	70%	57%

The effect of TEG on the slab length is often contradictory in the literature. For instance, a slight increase in slab length upon TEG incorporation has been reported for CoMo catalysts.[27,30] Other studies[34,35] reported a decrease in slab length upon TEG incorporation, attributed to an increase in the Co/Mo edge ratio, with more Co atoms on the edges, limiting MoS_2 growth.[34] Our results show that TEG has a weak effect on MoS_2 slab size with respect to non-additivated dried catalysts, while a slight homogenization of the stacking number and slab length can be attributed to the presence of the organic additive.

Catalytic activity of the model systems: thiophene hydrodesulfurization reaction

The catalytic activity of the model dried CoMoP and CoMoP-TEG catalysts was evaluated by a thiophene hydrodesulfurization reaction in batch conditions for a 24-hour reaction span. Their activity is compared to that of calcined CoMo catalysts reported in Ref.[23] (Fig. 7).

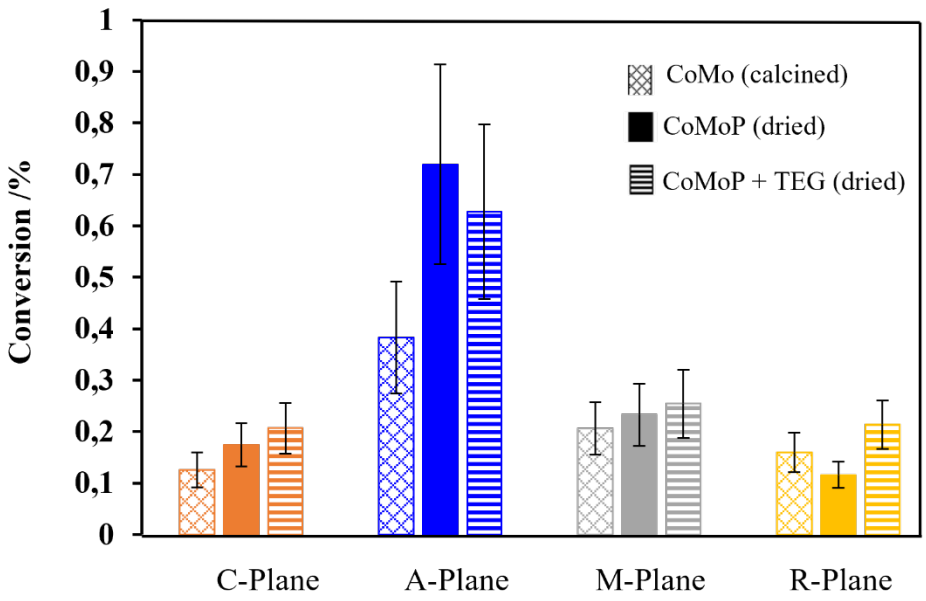

Figure 7. Thiophene conversion towards hydrodesulfurization products for model calcined CoMo[23] as well as dried CoMoP and CoMoP + TEG HDS catalysts supported on the C(0001), A($11\bar{2}0$), M($10\bar{1}0$) and R($1\bar{1}02$) crystal planes of α-Al_2O_3 sulfided at 400 °C. Reaction conducted at 400 °C for 24 hours. Each catalyst exhibits the same exposed total area (four single crystals) and similar metal surface concentrations. Error bars of CoMoP and CoMoP-TEG samples correspond to the standard deviation over two to five measurements obtained for calcined CoMo catalysts.[23]

As seen in Fig. 7, A$(11\bar{2}0)$ plane-based catalysts clearly exhibit higher catalytic activity than C(0001), M$(10\bar{1}0)$ and R$(1\bar{1}02)$-based regardless of the formulation and thermal treatment, which confirms the higher intrinsic activity for catalysts supported on the former crystal plane, as previously discussed in Ref.[23]

When comparing calcined CoMo and dried CoMoP catalysts, Fig. 7 also shows that phosphorus incorporation and the absence of a calcination step (CoMoP) has a clear enhancing effect on the activity of A$(11\bar{2}0)$-based catalysts. A timid increase in activity is reported for C(0001) and M$(10\bar{1}0)$-based, and a slight decrease for R$(1\bar{1}02)$ plane-based catalysts with respect to calcined CoMo catalysts, although the difference in activity for these model catalysts is not large enough to be conclusive.

The effect of TEG on the activity of C(0001), M$(10\bar{1}0)$ and R$(1\bar{1}02)$-based catalysts remains moderate as well, since the reported activity increase with respect to dried CoMoP (dried) counterparts reported in Fig. 7 remain within experimental uncertainty. However, a slight decrease in activity can be noted for TEG-additivated A$(11\bar{2}0)$-based catalysts (with respect to its dried CoMoP counterpart), suggesting a detrimental effect of TEG on the performance of the most active system.

In order to correct the conversion values for the total moles of active sites (edge and corner Mo sites of MoS_2 slabs), a normalized conversion was calculated (φ, Table 5) for the different model catalysts according to the procedure described in Section 2.4.

Table 5. Normalized conversion (φ, per mol Mo edge/corner sites) for the thiophene hydrodesulfurization reaction carried out on model catalysts supported on the C(0001), A$(11\bar{2}0)$, M$(10\bar{1}0)$ and R$(1\bar{1}02)$ crystal planes of α-Al_2O_3 at 400 °C

φ / 10^{-6} (mol edge site)$^{-1}$	C(0001)	A$(11\bar{2}0)$	M$(10\bar{1}0)$	R$(1\bar{1}02)$
CoMo (Calcined)	1.8	6.0	3.4	2.1
CoMoP	2.4	10.4	3.3	2.1
CoMoP-TEG	2.9	7.6	3.3	3.4

As seen in Table 5, the trends of normalized conversions coincide with the raw conversion values shown in Fig. 7, confirming that the trends in activity are related to

differences in intrinsic activity for each orientation. It can be seen from Table 5 that TEG incorporation improves the intrinsic activity of model catalysts supported on C(0001), A$(11\bar{2}0)$ and R$(1\bar{1}02)$-based catalysts with respect to calcined CoMo catalysts,[23] while it remains unchanged for the case of M$(10\bar{1}0)$-based ones.

The effect of TEG on the intrinsic activity is less evident when comparing these results with the ones obtained with the dried CoMoP formulation. For instance, while both C(0001) and R$(1\bar{1}02)$-based catalysts show timid improvements in intrinsic activity, it remains unchanged for M$(10\bar{1}0)$-based ones and it even decreases for those supported on the A$(11\bar{2}0)$ plane.

The selectivity chart of dried CoMoP-TEG (Fig. 8) and dried CoMoP (Supporting information) shows the same selectivity trend as CoMo catalysts:[23] 1-butene >1,3-butadiene ≃ trans-2-butene > cis-2-butene > n-butane for C(0001), M$(10\bar{1}0)$ and R$(1\bar{1}02)$-based catalysts planes with slight variations for A$(11\bar{2}0)$-based ones. It is worth remarking that the final products of thiophene hydrodesulfurization are 1-butene and 2-butene isomers (and n-butane if further hydrogenation occurs). On the contrary, 1,3-butadiene is the primary product of the direct desulfurization pathway (DDS). C(0001), M$(10\bar{1}0)$ and R$(1\bar{1}02)$-based catalysts display roughly 25% of 1,3-butadiene as the total yield, indicating that DDS pathway occurs at similar rates for these model catalysts. In the case of the A$(11\bar{2}0)$-based model catalysts, the comparatively higher conversion pushes the reaction towards the 1- and 2-butene isomers in detriment of 1,3-butadiene concentration, maybe indicating the hydrogenation pathways in thiophene HDS is enhanced for this surface.

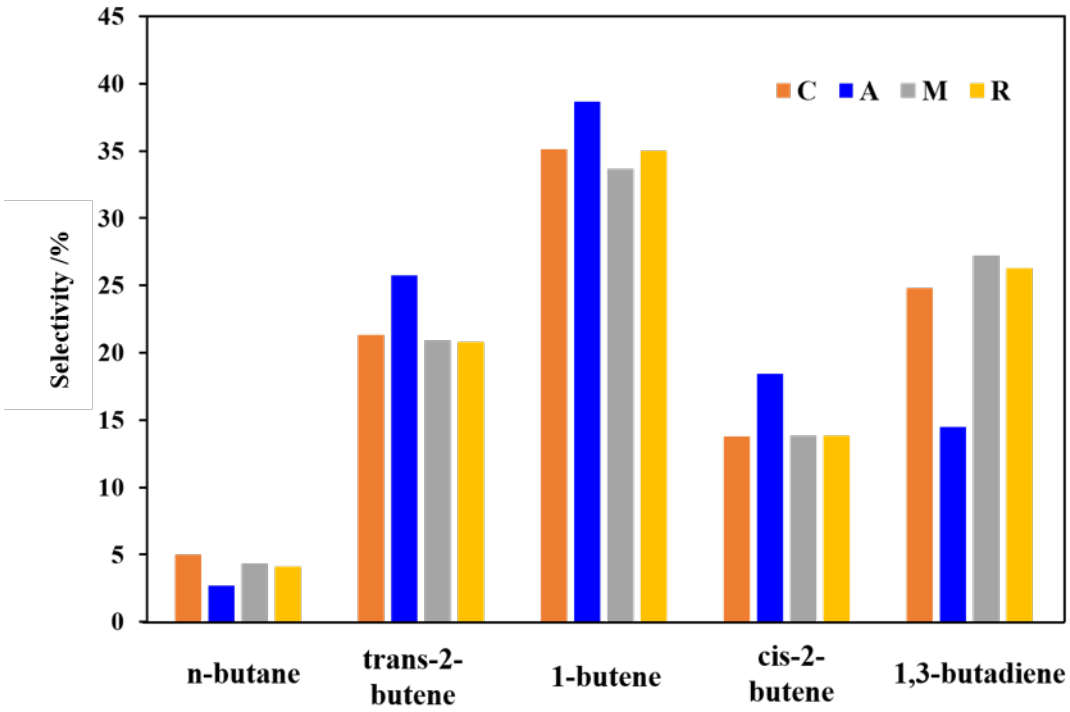

Figure 8. Selectivity of the model dried CoMoP + TEG model catalysts supported on the A$(11\bar{2}0)$, C(0001), M$(10\bar{1}0)$ and R$(1\bar{1}02)$ crystal planes of α-Al_2O_3 sulfided at 400 °C for a thiophene hydrodesulfurization reaction conducted at 400 °C for 24 hours.

Discussion: active phase-support interactions and catalytic activity

Background

The catalytic activity results displayed in the previous section clearly show a higher intrinsic activity for A$(11\bar{2}0)$-based catalysts with respect to M$(10\bar{1}0)$, R$(1\bar{1}02)$ and C(0001)-based ones. The origin of the observed trends in surface-dependent activity were previously discussed in Ref.[23]

Indeed, it was proposed that high activity emerged from a compromise between weak and strong active phase-support interactions (the latter associated respectively to C(0001) and R$(1\bar{1}02)$-based catalysts respectively), resulting in a high activity for catalysts displaying interactions of intermediate strength. While the exact cause of this compromise is yet to be resolved, we proposed a hypothesis to explain such behavior: the effect of metal-support interaction on metal-sulfur (M-S) bond energy at CoMoS edges. It has been shown initially that a volcano-type curve is obtained when plotting the activity of different bulk transition metal sulfides as a function of their M-S bond energies.[36,37] Moreover, regarding supported catalysts, by comparing anatase and γ-alumina, the work of Arrouvel *et al*.[38] has refined this concept suggesting that, for given transition metal sulfides, strong metal-support interactions will decrease M-S bond energy. In that sense, we can extent also this concept to the different surface orientations of a given oxide phase (α-alumina) and we hypothesized that an optimal M-S energy (leading to maximized activity) is attained by metal-support interactions of intermediate strength such as those found on A$(11\bar{2}0)$ and (to a lesser extent) M$(10\bar{1}0)$-based catalysts.

Activity of CoMoP (dried) model catalysts

The hypothesis invoked in Section 4.1 remains valid for dried CoMoP catalysts since the ranking in catalytic activity among the various surfaces is the same as the one observed for calcined CoMo catalysts. Therefore, we suggest that the results shown in Fig. 7 are an

alternative version of a volcano-shaped curve, while considering metal-support interactions as a key descriptor of the catalytic activity through a direct influence on M-S bond energy, according to the Sabatier principle.

Moreover, as shown in the results, the absence of the calcination step and incorporation of P in the catalyst formulation (dried CoMoP) further improved the raw catalytic activity of A$(11\bar{2}0)$-based catalysts with respect to calcined CoMo catalysts. Indeed, a sizable increase is noted for CoMoP-A$(11\bar{2}0)$-based catalysts, which display 1.9-times the conversion measured for calcined CoMo catalysts (Fig. 7). Such an increase can be directly correlated to a 73% increase in the normalized conversion (Table 5) reported for catalysts prepared with the CoMoP (dried) formulation with respect to the CoMo (calcined one) and also to higher sulfidation rates increasing the number of active sites.

While the sulfidation extent and lateral dispersion (slab length) were considered in the calculation of the intrinsic activity, another active phase descriptor may account for the improved activity observed in A$(11\bar{2}0)$-based catalysts: slab stacking. For instance, the absence of calcination in CoMoP catalysts brings a significant decrease in crystallite stacking (47% single slabs) with respect to CoMo catalysts (26 % single slabs) as evidenced by TEM measurements (Table 4). According to some authors, for basal-bonded CoMoS crystallites, the increase in single CoMoS slabs would imply a rise in more accessible sites[39,40]. Hence, part of the enhanced activity in dried CoMoP catalysts may arise from the predominance of single CoMoS slabs. However, the better activity of single vs. multi-stacked slabs is still highly debated and must not be taken for granted.[10,39–43]

The intrinsic activity of CoMoP-C(0001)-based catalysts rose by 33% with respect to calcined CoMo ones (Table 5), which could be also explained by the reduction in multi-stacked slabs, as we evoked for A$(11\bar{2}0)$-based catalysts. On the contrary, the intrinsic activities of M$(10\bar{1}0)$ and R$(1\bar{1}02)$-based catalysts remain unchanged with respect to their calcined CoMo counterparts. Nevertheless, it is difficult to draw a definite conclusion for these surfaces due to the rather small variations in raw conversions between calcined CoMo and dried CoMoP formulations observed for C(0001), M$(10\bar{1}0)$ and R$(1\bar{1}02)$-based catalysts. Further measurements should be undertaken in order to confirm the trends presented in this work.

Perhaps the most important conclusion that can be drawn from the obtained results is that the influence exerted by the support on the activity is clearly predominant over that of thermal

treatment or dopant incorporation. This assertion is based not only on the fact that A$(11\bar{2}0)$-based catalysts highly overperform over C(0001), M$(10\bar{1}0)$ and R$(1\bar{1}02)$-based ones regardless of the formulation, but also by the fact that a different thermal treatment and P incorporation has a much larger effect on A$(11\bar{2}0)$-based systems than for the other surface orientations.

Effect of TEG incorporation on the activity of CoMoP (dried) catalysts

When compared to dried CoMoP catalysts, TEG additivation has two main effects which are observed at different sulfidation temperatures. At 300 °C sulfidation, TEG incorporation allows higher sulfidation extents with respect to CoMoP catalysts regardless of the crystal orientation. At 400 °C, TEG incorporation tends to level out differences in the genesis of the active phase with respect to CoMoP catalysts, e.g. similar sulfidation degree, stacking number and slab length. Nevertheless, some other features remain modified at 400°C sulfidation: a very slight reduction in the stacking number (except for R$(1\bar{1}02)$-based catalysts), suggesting an overall increase in dispersion related to crystallite height, and higher Co promotion extents regardless of the crystal plane (Fig. 2).

At this point, it is worth highlighting that differences in both sulfidation extents and dispersion trends among CoMoP-TEG model catalysts are more significant at 300 °C than at 400 °C. In that sense, we could expect higher differences in hydrodesulfurization activity at 300 °C among CoMoP-TEG systems based on the results from Glasson *et al*.[44] although this could not be verified due to the low activity of model catalysts at this reaction temperature.

Table 5 indicates that the intrinsic activity (normalized conversion) at 400°C of CoMoP-TEG model catalysts supported on the A$(11\bar{2}0)$ plane decreases with respect to the dried CoMoP formulation. This decrease may be explained by a detrimental modification of the optimal active phase properties for the A$(11\bar{2}0)$-based catalysts (Mo-S bond energy). In other words, an optimum in metal/support interactions might have been reached within the dried CoMoP formulation while TEG incorporation might have destabilized such optimum. Nonetheless, the raw conversion of CoMoP-TEG model catalysts is still 1.7-times higher than that of their calcined CoMo counterparts, mostly due to enhanced Mo sulfidation and Co promotion extent.

On the contrary, CoMoP-TEG model catalysts supported on the C(0001), M$(10\bar{1}0)$ and R$(1\bar{1}02)$ crystal planes show a modest increase in raw conversion with respect to dried CoMoP catalysts. This is also true for their intrinsic activity, except for M$(10\bar{1}0)$-based catalysts, which show constant activity. Such behavior might emerge from an optimization of metal/support interactions upon TEG additivation with respect to dried CoMoP catalysts leading to an improvement in Mo-S bond energy at the edges and enhanced promotion extents. Once again, such conclusions are limited by the close conversion values observed for both formulations. The same conclusion drawn above regarding the predominance of surface effects over other parameters can be drawn for TEG-additivated systems: the influence of the organic additive remains weak compared to the one exerted by surface sorption sites, which will define activity trends regardless of the thermal treatment or additive incorporation.

Finally, in order to relate the results obtained for the α-Al_2O_3-based model system to the traditional γ-Al_2O_3 support, we must invoke the relationship among the crystal planes of both polymorphs. By invoking the parallelism among surface sites already described in refs [20-24], it is possible to estimate the intrinsic activities for CoMo catalysts supported on different γ-Al_2O_3 facets based on a proposed α-/γ- analogy [20-24]. These relationships are summarized and schematized in Fig. 9.

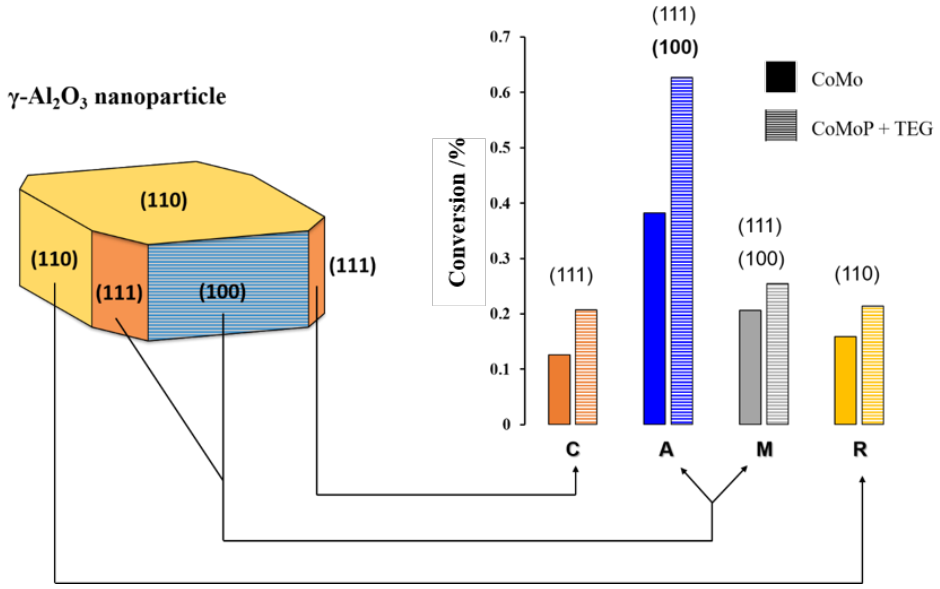

Figure 9. Schematic representation of the surface-dependent conversion of the different facets that make up the γ-Al_2O_3 nanoparticle (Digne *et al.*[45]) obtained by transposition of the results obtained with the model α-Al_2O_3-based model catalysts prepared with CoMo (calcined) and CoMoP-TEG (dried) formulations.

The scheme in Fig. 9 suggests that a γ-Al_2O_3-supported catalyst displaying surface sites from the (100) crystal plane would exhibit higher catalytic activity than others supported on the (110) and (111) planes.

Engineering γ-Al_2O_3 to exhibit preferentially these surface sites could confirm the relationships and trends shown in Fig. 9. In addition, it could lead to a new generation of HDT catalysts based on specialized support design synthesized to provide optimal and intermediate active phase-support interactions.

Conclusions

A surface science approach was adopted in this work in order to gain insight into the effects of phosphorus doping and TEG addition on the genesis of the promoted CoMo active phase and its catalytic activity. Four crystal orientations of α-Al_2O_3 were used as model planar supports to provide controlled speciation of surface sorption sites (A$(11\bar{2}0)$, C(0001), M$(10\bar{1}0)$ and R$(1\bar{1}02)$ planes). These surfaces hold surface Al-OH groups that can also be identified on the different γ-Al_2O_3 facets.

The influence of the calcination step on the sulfidation and Co promotion extents was assessed in CoMoP catalysts at first. It was found that calcination decreases both Mo sulfidation degree and Co promotion extent which is explained by enhanced metal/support interactions with respect to dried catalysts.

The effect of TEG on the genesis of the promoted active phase was also studied for dried (not calcined) CoMoP formulations. It was found that CoMoP-TEG catalysts display higher Mo sulfidation extents and dispersion levels than dried CoMoP ones at 300 °C sulfidation, while such differences are leveled out at 400 °C. Higher Co promotion extents were observed upon TEG incorporation as well, due to enhanced sulfidation degrees and probably also due to a more efficient decoration of MoS_2 slabs, presumably as a consequence of the preservation of the $PCoMo_{11}O_{40}^{7-}$ heteropolyanion during the drying step.

The catalytic activity of model dried CoMoP and CoMoP-TEG catalysts was tested in a thiophene hydrodesulfurization reaction in batch configuration. The conversion trends revealed a surface-dependent activity: A$(11\bar{2}0)$ > > M$(10\bar{1}0)$ > R$(1\bar{1}02)$, C(0001), confirming that A$(11\bar{2}0)$ plane-based catalysts hold intrinsically higher activity than the other model catalysts. The high activity of the A$(11\bar{2}0)$ plane-based catalysts is assigned to intermediate and optimal active phase-support interactions, which appear key to enhance HDS activity. Moreover, it is shown that the incorporation of P/TEG has an overall positive effect on the raw activity with respect to a traditional CoMo (calcined) formulation. Such observation is explained both by an evident increase in the normalized conversion, which indicates a higher intrinsic activity and by enhanced metal sulfidation due to weakened active phase-support interactions, leading to an increase in the number of active sites available for hydrodesulfurization.

However, this work also demonstrates that the surface effect on catalytic activity appears to be predominant over the effect of P doping or TEG additivation.

Relating the results obtained on model systems to γ-Al_2O_3-supported real catalysts leads to a better rationalization of the surface-dependent effect of dopants (phosphorus) and additives (TEG) on the genesis of the active phase and catalytic activity of industrial catalysts.

Experimental Section

Preparation of model CoMoP and CoMoP-TEG/α-Al_2O_3 catalysts

Model HDS catalysts were prepared by impregnating a precursor solution on the top surface of α-Al_2O_3 single crystals of four different orientations: C(0001), A($11\bar{2}0$), M($10\bar{1}0$), and R($1\bar{1}02$). The single crystals had dimensions of 1.0 cm x 1.0 cm x 0.50 mm (1cm^2 surface area) and were purchased from MaTecK Material Technologie & Kristalle GmbH (A and R orientations) and SurfaceNet GmbH (C and M orientations) (Germany). Prior to precursor solution deposition, the single crystals were subject to a chemical cleaning procedure detailed in a previous contribution.[23]

CoMoP model catalysts were prepared by drop-casting 100 µL of a solution containing all precursors required for this catalyst formulation (co-impregnation) on the single crystals.[23] Mo and P were incorporated from a mother phospho-molybdic solution with a molar P/Mo ratio of 0.57 (synthesis described in Ref.[24]) and Co was incorporated as $Co(NO_3)_2$. The solutions were prepared with a Co/Mo molar ratio of 0.5.[46,47] The concentration of the precursor solutions was $6.8 \cdot 10^{-6}$ $mol.L^{-1}$ in Mo and $3.4 \cdot 10^{-6}$ $mol.L^{-1}$ in Co, in order to ensure a surface concentration of ~ 4.0 atoms·nm^{-2} of molybdenum and ~ 2.0 atoms·nm^{-2} of cobalt. These loadings would correspond to ~16 wt% MoO_3 and ~5 wt% CoO for a traditional 200 $m^2 \cdot g^{-1}$ γ-Al_2O_3 powder support. The CoMoP-TEG precursor solution was obtained after adding the organic additive to the mother CoMoP precursor solution described above, with a molar TEG/Mo ratio of 0.5. After drop-casting the solution, the wafers were dried at ambient temperature under vacuum.

For CoMoP systems, two identical model catalysts per crystal plane were prepared. After drying, one set underwent calcination (450 °C, 2h in air), while the other was left in the dried state. As usually done to enhance the organic additive effect, CoMoP-TEG model catalysts were not subjected to calcination.

Sulfidation of model catalysts

The model catalysts were sulfided (activated) in a glass reactor (≈ 27 mL). The sulfidation scheme proceeded as follows: first, the system was purged with 2 NL·h^{-1} argon flow for five minutes. Gas phase sulfidation began at atmospheric pressure under a 2 NL·h^{-1} 15% mol H_2S/H_2

gas flow before heating the sulfidation cell at 5 °C/min until reaching the target temperature (300 or 400 °C). This temperature was kept constant for 2 h before switching to Ar at 2 $NL \cdot h^{-1}$ and cooling down in a 15 °C/min descending ramp down to 150 °C. Subsequently, the argon atmosphere was kept at this temperature for 1 h. Finally, the system reached ambient temperature under argon flux. After the sulfidation cycle was completed, the activated catalysts were kept under argon atmosphere inside a hermetic storage device.

Characterization of model catalysts

X-ray photoelectron spectroscopy

XPS spectra were obtained with an Omicron (ESCA+) instrument using a monochromatic Al X-ray source (hν = 1486.6 eV) with an accelerating voltage of 14 kV and a current of 20 mA (with an overall energy resolution of 0.8 eV). The spectra were collected at a takeoff angle of 90° under a pressure below $1 \cdot 10^{-9}$ mbar at ambient temperature. The surveyed XPS regions were C1s, O1s, Al2p, Mo3d, Co2p, and S2p. The obtained spectra for each region were calibrated based on the C1s photopeak of adventitious carbon at 284.6 eV.[46,47] After spectra collection, the mathematical decomposition of the different contributions was performed using the Casa XPS software.[48] Spectral decomposition of the Mo3d, S2s, S2p, and Co2p regions was carried out by following the premises established by Gandubert et al.[46,47] and a standardized procedure based on a common set of binding energy and FWHM restrictions was imposed on every spectrum for the sake of consistency. More information regarding XPS analysis of model catalysts can be found in Ref. [23].

The Mo3d XPS spectra of sulfided Mo-based catalysts were decomposed into three contributions: MoO_3, MoO_xS_y, and MoS_2. By expressing the total Mo surface density as a sum of the areas corresponding to the three Mo contributions, the relative percentage of MoS_2 with respect to the rest of Mo species, was calculated according to:

$$\%\,MoS_2 = \frac{A_{MoS_2}}{A_{MoS_2} + A_{MoO_xS_y} + A_{MoO_3}} \times 100 \qquad (2)$$

$\%MoS_2$ will be referred to as sulfidation degree.

The Co2p XPS region was also decomposed into three contributions: Co^{2+}, Co_9S_8, and CoMoS. The relative percentage of Co incorporated at the edges of MoS_2 (CoMoS phase) on each model catalyst was calculated according to Eq. 3 and will be referred to as the promotion extent.

$$\% \text{ CoMoS} = \frac{A_{CoMoS}}{A_{CoMoS} + A_{Co_9S_8} + A_{Co^{2+}}} \times 100 \qquad (3)$$

Sample transfer from the hermetic storage recipient to the XPS chamber was carried out via a rapid procedure (less than 1 minute). It was verified that samples did not undergo significant re-oxidation during the transfer.

Atomic force microscopy (AFM)

Model catalysts were evaluated by AFM in the sulfide phase (300 °C sulfidation) using a Nanoscope VIII Multimode AFM (Bruker, USA) through peak force tapping mode at 2 kHz resonance frequency. Every analyzed sample was imaged at two or three different locations on the surface. The probing tips were purchased from Bruker (United States). The model was a SCANASYST-AIR silicon tip on nitride lever with a force constant of 0.4 N/m. The reported surface roughness corresponds to the root mean square roughness (R_{rms}), which indicates the average of all deviations from the surface baseline. These deviations are interpreted as clusters/particles of catalyst precursors adsorbed on the crystal surface. All R_{rms} values are reported within ± 0.01 nm accuracy.

Transmission electron microscopy (TEM)

TEM images were collected with a JEOL 2010 microscope operating at 200 kV. The average MoS_2 slab lengths and stacking numbers were obtained by measuring no less than 200 slab clusters per sample for statistical purposes. The slabs were quantified using the ImageJ 1.45 software.[49] TEM samples were prepared by scraping the top surface of the wafers with a stainless-steel razor blade in order to recover the upmost alumina surface fragments, thin enough to allow electron microscopy analysis. The fragments were suspended into a drop of absolute ethanol, which was then deposited on a carbon-coated Cu-grid. The slab length for each MoS_2 slab was obtained by manually measuring the visible darkened stripes that

contrasted with the lighter α-Al_2O_3 background. The stacking number was determined by quantification of visible stripe layers for every MoS_2 cluster.

Grazing-incidence X-ray absorption spectroscopy (GI-XAS)

The model planar catalysts were characterized by GI-XAS (grazing-incidence X-ray absorption spectroscopy) in fluorescence mode with a Canberra 35 elements solid-state Ge detector at the Co K edge (7.7 keV) on the SAMBA beamline at SOLEIL (Saint-Aubin, France).[50] Details regarding the analysis setup can be found in Ref. [23].
Each model catalyst was first sulfided at 300 °C and then analyzed in parallel configuration with respect to the electric filed vector. Processing of the XAS data was carried out with the Demeter package.[51] The reference Co_9S_8 XAS spectrum was kindly provided by V. Briois (SOLEIL synchrotron) following a temperature-programmed method reported by Plais et al.[28]

Thiophene hydrodesulfurization

The performance of the model catalysts was assessed by a thiophene hydrodesulfurization reaction in the gas phase under batch configuration. The HDS reaction took place at 400 °C for 24 h at atmospheric pressure (1 bar). The reactor used for the catalytic tests was the same as the one used for sulfidation (section 2.2). Four identical samples (single crystals) of each model catalyst (preparation is detailed in Section 2.1) were first sulfided and then set up for the reaction, according to the procedure described in Ref.[23] The concentration of thiophene and hydrodesulfurization products (hydrocarbons) was obtained through gas chromatography (GC). The GC column allowed the identification of five products of the thiophene hydrodesulfurization reaction: n-butane, trans-2-butene, 1-butene, cis-2-butene, and 1,3-butadiene. In order to determine their concentrations, GC response factors were initially obtained for thiophene and 1,3-butadiene. The response factor for the rest of the hydrocarbon products was assumed to be identical as the one of 1,3-butadiene.[23,52]

The conversion after 24 h in batch mode was defined as:

$$X_{thiophene} = \frac{\sum_n C_i}{\sum_n C_i + C_{thiophene\ t=24h}} \quad (6)$$

where C_i is the concentration (in ppm) of product "i" and $C_{thiophene\ t=24h}$ is the remaining thiophene concentration after 24 h of reaction. The conversion was defined from product concentration instead of the difference between the final and initial thiophene concentration due to the very low conversion which is of the order of magnitude of the error in thiophene concentration between measurements.

A normalized conversion was determined instead of the traditional TOF (large error difference between the reactor volume and the GC area peaks) in order to compare samples with respect to the number of active sites. The conversion obtained by Eq. (6) was normalized by the number of Mo moles in edges and corners of MoS_2 slabs (active sites), following the slab geometry model of S. Kasztelan.[6] A detailed description of this calculation is available in Ref. [23] and the normalized φ is given by:

$$\varphi/(\text{mol Mo edge} + \text{corners}) = \frac{X}{\text{mole Mo} \cdot \%\ MoS_2 \cdot \overline{D}} \quad (7)$$

where X is the conversion, (mole Mo) is the total number of surface Mo (mol.) determined by XPS, % MoS_2 the sulfidation degree determined by XPS, and $\overline{D}$ the average lateral dispersion (see Supporting Information for calculation details).

After each reaction cycle, the product selectivity was also calculated according to the following expression:

$$S_i = \frac{C_i}{\sum_i C_i} \cdot 100\% \quad (11)$$

where S_i is the selectivity of product "i" and C_i the concentration of product "i".

Acknowledgements

We gratefully thank Cyril Thomas for his precious help in the development of the catalytic test, Sandra Casale for her support with TEM experiments and Anne-Lise Taleb for her assistance on data treating of TEM images. We also thank Christophe Méthivier for his support in XPS data acquisition and analysis. We thank Valérie Briois for providing reference Co K-edge XANES spectra. Finally, we also acknowledge SOLEIL Synchrotron for provision of synchrotron radiation facilities (proposal 20190184), in particular Emiliano Fonda and Guillaume Alizon for their scientific and technical assistance throughout the experiences carried out at SAMBA beamline at SOLEIL.

Keywords

Hydrotreating, Alumina, Surface-science, CoMo catalysts, Volcano plot

References

[1] UN Environment Programme, “The Global Sulphur Progress Tracker". Can be found under https://www.unep.org/es/node/24962. Consulted on January 11th 2021.

[2] European Parliament, *Off. J. Eur. Union* **2009**, L140/88-L140/113.

[3] H. Toulhoat, P. Raybaud, *Catalysis by Transition Metal Sulphides : From Molecular Theory to Industrial Application*, Editions TECHNIP, **2013**.

[4] A. Gruia, *Handb. Pet. Process.*, Springer Netherlands, Dordrecht, **2008**, 321–354.

[5] E. Payen, R. Hubaut, S. Kasztelan, O. Poulet, J. Grimblot, *J. Catal.* **1994**, *147*, 123–132.

[6] S. Kasztelan, H. Toulhoat, J. Grimblot, J. P. Bonnelle, *Appl. Catal.* **1984**, *13*, 127–159.

[7] C. Wivel, B. S. Clausen, R. Candia, S. Mørup, H. Topsøe, *J. Catal.* **1984**, *87*, 497–513.

[8] D. Laurenti, B. Phung-Ngoc, C. Roukoss, E. Devers, K. Marchand, L. Massin, L. Lemaitre, C. Legens, A.-A. Quoineaud, M. Vrinat, *J. Catal.* **2013**, *297*, 165–175.

[9] T. K. T. Ninh, L. Massin, D. Laurenti, M. Vrinat, *Appl. Catal. A Gen.* **2011**, *407*, 29–39.

[10] L. van Haandel, G. M. Bremmer, E. J. M. Hensen, T. Weber, *J. Catal.* **2016**, *342*, 27–39.

[11] L. van Haandel, G. M. Bremmer, E. J. M. Hensen, T. Weber, *J. Catal.* **2017**, *351*, 95–106.

[12] D. Nicosia, R. Prins, *J. Catal.* **2005**, *229*, 424–438.

[13] J. Mazurelle, C. Lamonier, C. Lancelot, E. Payen, C. Pichon, D. Guillaume, *Catal. Today* **2008**, *130*, 41–49.

[14] T. S. Nguyen, S. Loridant, L. Chantal, T. Cholley, C. Geantet, *Appl. Catal. B Environ.* **2011**, *107*, 59–67.

[15] R. Prins, *J. Catal.* **2020**, *392*, 336–346.

[16] J. V. Lauritsen, S. Helveg, E. Lægsgaard, I. Stensgaard, B. S. Clausen, H. Topsøe, F. Besenbacher, *J. Catal.* **2001**, *197*, 1–5.

[17] J. V. Lauritsen, M. V. Bollinger, E. Lægsgaard, K. W. Jacobsen, J. K. Nørskov, B. S. Clausen, H. Topsøe, F. Besenbacher, *J. Catal.* **2004**, *221*, 510–522.

[18] J. C. Muijsers, T. Weber, R. M. Vanhardeveld, H. W. Zandbergen, J. W. Niemantsverdriet, *J. Catal.* **1995**, *157*, 698–705.

[19] Y. Sakashita, *Surf. Sci.* **2001**, *489*, 45–58.

[20] C. Bara, L. Plais, K. Larmier, E. Devers, M. Digne, A.-F. Lamic-Humblot, G. D. Pirngruber, X. Carrier, *J. Am. Chem. Soc.* **2015**, *137*, 15915–15928.

[21] C. Bara, A. F. Lamic-Humblot, E. Fonda, A. S. Gay, A. L. Taleb, E. Devers, M. Digne, G. D. Pirngruber, X. Carrier, *J. Catal.* **2016**, *344*, 591–605.

[22] C. Bara, E. Devers, M. Digne, A.-F. Lamic-Humblot, G. D. Pirngruber, X. Carrier, *ChemCatChem* **2015**, *7*, 3422–3440.

[23] R. Garcia de Castro, E. Devers, M. Digne, A. Lamic- Humblot, G. D. Pirngruber, X. Carrier, *J. Catal.* **2021**, *403*, 16-31

[24] R. Garcia de Castro, J. Bertrand, B. Rigaud, E. Devers, M. Digne, A. Lamic-Humblot, G. Pirngruber, X. Carrier, *Chem. – A Eur. J.* **2020**, *26*, 14623–14638.

[25] L. van Haandel, G. M. Bremmer, E. J. M. Hensen, T. Weber, *J. Catal.* **2017**, *351*, 95–106.

[26] N. C. G. Jacob, *Int. J. Res. Eng. Technol. 03*, 346–350.

[27] V. Costa, B. Guichard, M. Digne, C. Legens, P. Lecour, K. Marchand, P. Raybaud, E. Krebs, C. Geantet, *Catal. Sci. Technol.* **2013**, *3*, 140–151.

[28] L. Plais, C. Lancelot, C. Lamonier, E. Payen, V. Briois, *Catal. Today* **2020**, *377*, 114-126.
[29] A. Gutiérrez-Alejandre, G. Laurrabaquio-Rosas, J. Ramírez, G. Busca, *Appl. Catal. B Environ.* **2015**, *166–167*, 560–567.
[30] P. Mazoyer, C. Geantet, F. Diehl, C. Pichon, T. S. Nguyen, M. Lacroix, *Oil Gas Sci. Technol.* **2005**, *60*, 791–799.
[31] V. Costa, K. Marchand, M. Digne, C. Geantet, *Catal. Today* **2008**, *130*, 69–74.
[32] D. Nicosia, R. Prins, *J. Catal.* **2005**, *234*, 414–420.
[33] J. A. Bergwerff, L. G. A. van de Water, T. Visser, P. de Peinder, B. R. G. Leliveld, K. P. de Jong, B. M. Weckhuysen, *Chem. - A Eur. J.* **2005**, *11*, 4591–4601.
[34] A. Pimerzin, A. Mozhaev, A. Varakin, K. Maslakov, P. Nikulshin, *Appl. Catal. B Environ.* **2017**, *205*, 93–103.
[35] J. Escobar, M. C. Barrera, J. A. Toledo, M. A. Cortés-Jácome, C. Angeles-Chávez, S. Núñez, V. Santes, E. Gómez, L. Díaz, E. Romero, J. G. Pacheco, *Appl. Catal. B Environ.* **2009**, *88*, 564–575.
[36] H. Toulhoat, P. Raybaud, *J. Catal.* **2003**, *1-2*, 63–72.
[37] H. Toulhoat, P. Raybaud, *Catal. Sci. Technol.* **2020**, *10*, 2069–2081.
[38] C. Arrouvel, M. Breysse, H. Toulhoat, P. Raybaud, *J. Catal.* **2005**, *232*, 161–178.
[39] H. Shimada, *Catal. Today* **2003**, *86*, 17–29.
[40] Y. Araki, K. Honna, H. Shimada, *J. Catal.* **2002**, *207*, 361–370.
[41] G. Berhault, M. Perez De la Rosa, A. Mehta, M. J. Yácaman, R. R. Chianelli, *Appl. Catal. A Gen.* **2008**, *345*, 80–88.
[42] B. Hinnemann, J. K. Nørskov, H. Topsøe, *J. Phys. Chem. B,* **2005**, 109, 6, 2245-2253.
[43] S. Eijsbouts, L. C. A. van den Oetelaar, R. R. van Puijenbroek, *J. Catal.* **2005**, *229*, 352–364.
[44] C. Glasson, C. Geantet, M. Lacroix, F. Labruyère, P. Dufresne, *Catal. Today* **1998**, *45*, 341–346.
[45] M. Digne, P. Sautet, P. Raybaud, P. Euzen, H. Toulhoat, *J. Catal.* **2004**, *226*, 54–68.
[46] A. D. Gandubert, C. Legens, D. Guillaume, S. Rebours, E. Payen, *Oil Gas Sci. Technol. - Rev. l'IFP* **2007**, *62*, 79–89.
[47] A. D. Gandubert, C. Legens, D. Guillaume, E. Payen, *Surf. Interface Anal.* **2006**, *38*, 206–209.
[48] Casa software Ltd, **2009**, 342.
[49] C. A. Schneider, W. S. Rasband, K. W. Eliceiri, *Nat. Methods* **2012**, *9*, 671–5.
[50] V. Briois, E. Fonda, S. Belin, L. Barthe, C. La Fontaine, F. Langlois, M. Ribbens, F. Villain, UVX 2010 - 10e Colloque sur les Sources Cohérentes et Incohérentes UV, VUV et X ; Applications et Développements Récents (2011) 41-47.
[51] B. Ravel, M. Newville, in *J. Synchrotron Radiat.*, International Union Of Crystallography, **2005**, pp. 537–541.
[52] A. J. Andreatch, R. Feinland, *Anal. Chem.* **1960**, *32*, 1021–1024.

Table of contents

The effect of phosphorus doping and triethylene glycol (TEG) incorporation on the genesis of the CoMoS phase of model HDT catalysts is assessed. The catalytic activity in thiophene hydrodesulfurization of the model catalysts prepared on α-Al_2O_3 single crystals with four orientations reveals a volcano-shaped curve with metal-support interactions as a key descriptor of the catalytic activity.